

## I-Band Asymptotic Giant Branch (IAGB) Stars: II. A First Estimate of their Precision and a Differential Zero Point<sup>\*</sup>

WENDY L. FREEDMAN,<sup>1,2</sup> BARRY F. MADORE,<sup>3,1</sup> TAYLOR HOYT,<sup>1</sup> IN SUNG JANG,<sup>1,2</sup> ABIGAIL J. LEE,<sup>1,2</sup> AND  
 KAYLA A. OWENS<sup>1</sup>

<sup>1</sup>*Department of Astronomy & Astrophysics, University of Chicago, 5640 South Ellis Avenue, Chicago, IL 60637*

<sup>2</sup>*Kavli Institute for Cosmological Physics, University of Chicago, 5640 South Ellis Avenue, Chicago, IL 60637*

<sup>3</sup>*Observatories of the Carnegie Institution for Science 813 Santa Barbara St., Pasadena, CA 91101*

### ABSTRACT

Hubble Space Telescope (HST) observations of 92 galaxies that have a strong showing of I-band Asymptotic Giant Branch (IAGB) stars in their color-magnitude diagrams (CMDs), are used to measure the relative offset between the mean apparent I-band magnitudes of the IAGB population and the corresponding apparent I-band magnitudes of the TRGB as measured in the same frames (and CMDs) of those individual galaxies. This first exploratory, large-sample comparison is independent of any extinction (foreground or internal) that may be shared by these two populations. The marginalized luminosity functions used to determine the modal value of the *IAGB* population are well fit by a single, symmetric Gaussian. The difference in the two apparent magnitudes (in the sense IAGB minus TRGB) is -0.589 mag, with a combined standard deviation of  $\pm 0.119$  mag. Adopting  $M_I = -4.05$  mag for the TRGB stars, the modal absolute magnitude of the *IAGB* is then calculated to be  $M_I(IAGB) = -4.64 \pm 0.12$  mag. The ensemble dispersion quoted above gives a standard error on the mean of  $\pm 0.012$  mag (based on the full sample of 92 galaxies). Independently, the three geometry-based zero points for I-band AGB stars are found (in Paper I) to be  $M_I = -4.49 \pm 0.003$  mag in the LMC (4204 stars),  $M_I = -4.67 \pm 0.008$  mag, for the SMC (916 stars) and  $M_I = -4.78 \pm 0.030$  mag for NGC 4258 (62 stars), leading to a global zero-point (weighted) average of  $< M_I > = -4.64 \pm 0.15$  mag (stat). The scatter found in the anchors is comparable to the scatter in the field sample discussed here, but the calibration sample is small. The application of this method to galaxies well outside of the Local Group, shows that these standard candles can readily be found and measured out to at least 9 Mpc, using already available archival data.

*Keywords:* cosmology: distance scale – cosmology: observations – galaxies: individual (LMC, SMC, NGC 4258) – galaxies: stellar content – stars: AGB and post-AGB

### 1. INTRODUCTION

In Madore et al. (2024; hereafter Paper I), we introduced *I-band AGB (IAGB)* stars as possible extragalactic distance indicators. These stars are closely related, but not identical to the *J-Branch AGB (JAGB)* stars of Weinberg & Nikolaev (2001), who drew attention to those stars as precision distance indicators, based on their near-infrared colors and magnitudes, as measured in the Large Magellanic Cloud (LMC). *JAGB* stars have subsequently been found to be excellent distance indicators in their own right (well beyond the LMC, see Freedman & Madore 2023, Lee 2023), and they are now a core part of the *Chicago Carnegie Hubble Program* (CCHP) using Cepheids, TRGB stars and now *JAGB* stars to determine three independent distances to each of the host galaxies being used to calibrate the absolute magnitudes of Type Ia supernovae (Freedman 2021) en route to the Hubble constant. As discussed in more detail in the Introduction to Paper I, *IAGB* stars are defined by their extremely red colors in the I vs (V-I) color-magnitude diagram (CMD). The blue cut-off is chosen to maximize the number of IAGB stars to the red contributing

Corresponding author: Wendy L. Freedman  
[wfreedman@uchicago.edu](mailto:wfreedman@uchicago.edu)

<sup>\*</sup> Based on observations made with the NASA/ESA Hubble Space Telescope, obtained at the Space Telescope Science Institute, which is operated by the Association of Universities for Research in Astronomy, Inc., under NASA contract NAS 5-26555.

to the measured luminosity function, while simultaneously minimizing contamination by the oxygen-rich population of precursor AGB stars found to the blue. In order to illustrate the effect of perturbing this blue cut-off around a nominal value, the three resulting luminosity functions are shown color-coded in the far right panels of Figures 3 through 10, below. It is our expectation that *IAGB* stars and *JAGB* stars are drawn from one and the same parent population, differing only in the contribution of (the bluest) stars still making the evolutionary transition from oxygen-rich to carbon-rich stars.

*IAGB* stars show the same uniquely identifiable colors and well-defined mean magnitudes as the *JAGB* stars, but the *IAGB* stars are defined at shorter wavelengths and bluer colors. This will prove to be an advantage for their discovery and application when *JWST* is considered, given the tighter point spread function (PSF) and finer angular resolution of the bluer filters available in the near-infrared imager, NIRCAM, on board *JWST*. NIRCAM’s F090W filter is a reasonably close match to the I-band (F814W) discussed here. In the application of the *JAGB* or *IAGB* methods at extreme distances, crowding in the outer disks will become a limiting factor, at which point the *IAGB* method will prevail.

## 2. ABSOLUTE CALIBRATION OF THE IAGB METHOD

In Paper I of this program we used the geometric distances to the LMC, SMC and NGC 4258 to provide three independent estimates of the zero point of the *IAGB* Method. Taken as an ensemble, these three anchor galaxies give  $M_I = -4.64 \pm 0.15$  mag (stat). Each of these calibrating galaxies has its own strengths and weaknesses. In combination, their inter-comparison may be informative as to the impact of their differing systematics and/or reveal errors in the adopted assumptions used in calibrating each of these datasets.

As pointed out in Paper I, to first order there is no measurable trend of the *IAGB* luminosity with metallicity, given that the *IAGB* zero points for the LMC and NGC 4258 (which have intermediate metallicities of 8.50 and 9.06 dex, respectively) fall on either side of the zero point derived for the SMC, which has the lowest metallicity ( $12 + \log(\text{O/H}) = 7.98$  dex)<sup>1</sup> of the three. In Section 4 of this paper we offer a first look at the possible level of influence of star formation history on the mode of the *IAGB* luminosity function, finding no evidence so far.

We now examine not only the zero point of the *IAGB* method, but also its precision and accuracy, including uncertainties due to sample size, differential reddening, variations in star formation history, regional crowding and metallicity. The scatter in Figure 1 puts a stringent upper limit on these “second parameters.”

## 3. A DIFFERENTIAL CALIBRATION OF THE IAGB ZERO POINT AND ITS DISPERSION

Here we undertake the differential comparison of the TRGB and I-band AGB (IAGB) methods, using a homogeneously reduced and self-consistently analyzed set of HST images for 92 relatively nearby, highly resolved galaxies. This sample consists of galaxies that have well-established *TRGB* distances and also show sufficient numbers of *IAGB* stars for the construction of robust I-band *AGB* luminosity functions.

The individual color-magnitude diagrams (CMD) and the resulting *IAGB* luminosity functions are shown in Figures 3 through 12. All of the data were retrieved from the *Extragalactic Distance Database* (EDD: Tully et al. 2009 <http://edd.ifa.hawaii.edu>). The entire collection of HST CMDs, for which EDD astronomers were able to obtain *TRGB* detections and measurements, were inspected by authors of this paper before special processing of the *IAGB* population. It needs to be noted that while all of the galaxies selected have I-band data (more specifically, [F814W] HST flight magnitude data) they do not all have data taken through the same blue-band filters with which a color is being formed. However, this is of little significance other than visibly shifting the blue color cut-off being adopted for a given galaxy, and used to define the redward *IAGB* sample. Given an adopted blue cut-off, stars redder than that value have then been projected onto the vertical I-band axis, binned and smoothed to form the continuous luminosity function seen in black in the right half of each panel. **To aid the reader, in judging the sensitivity of the luminosity function to changing the color cut-off, we also plot in red and blue, respectively, the luminosity functions formed after moving the color cut-off by  $\pm 0.1$  mag around the nominal value.** Because of the increasing density of stars approaching the “vertical” (O-type) AGB population situated to the blue, the red-colored luminosity function (having the largest amplitude) corresponds to the bluer cut-off (and the lower-amplitude, flanking luminosity function corresponds to the redder color cut-off). In most cases the modal value is stable to this level of variation in the method, but they are all shown on a galaxy by galaxy basis.

<sup>1</sup> Metallicities taken from the recent compilation of Madore & Freedman (2024) and references therein.

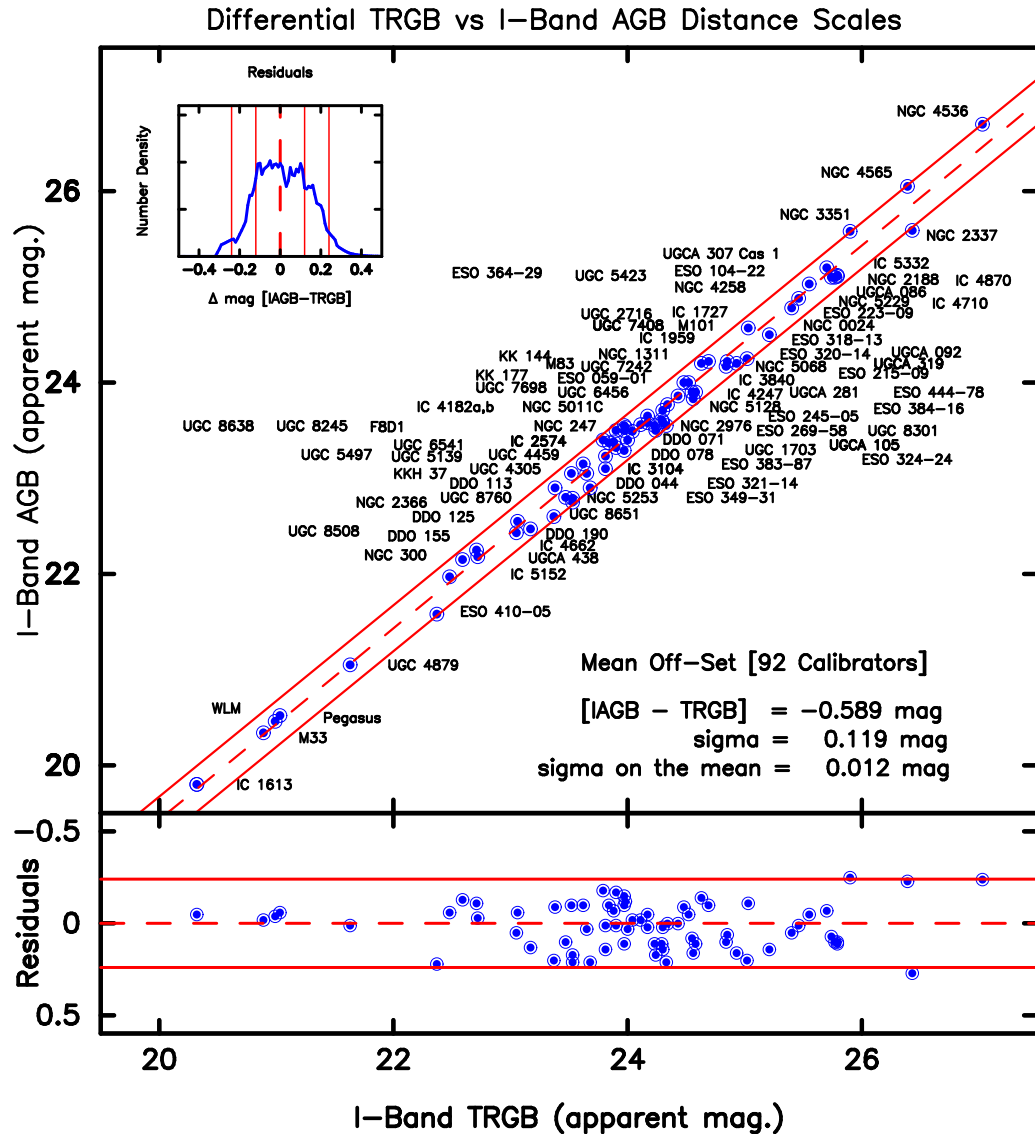


**Figure 1.** A differential comparison of the *TRGB* and *IAGB* distance scales. The apparent magnitude of the *TRGB* discontinuity is plotted on the horizontal axis. The apparent magnitude of the mode of the *IAGB* luminosity function is plotted on the vertical axis. The red dashed line has a slope of unity and has been fit to minimize the scatter of the data points around it. This minimization occurs at a value of  $-0.589 \pm 0.003$  mag (sigma on the mean) in the sense that the *IAGB* stars are brighter than the level of the *TRGB*. The measured inter-method scatter is  $\pm 0.119$  mag. The solid red lines are  $\pm$  two sigma bounds. The residuals are plotted as a function of the *IAGB* apparent I-band magnitude the lower panel. The marginalized histogram of residuals is shown in the small inset found in the upper left corner of the main plot.

In the right panels of Figures 3 through 14, a symmetric Gaussian (in blue) is then fit to the resulting luminosity function (in black) formed at the fiducial color cut-off. The fit is constrained by the peak in the observed luminosity function and by both of the wings of the distribution within 1-2 sigma of the peak. In most cases the fitted Gaussian underestimates the extended wings, which by choosing the mode, impose no bias one way or the other on the solution. That is, we are, in essence, simply measuring the dominant peak in the luminosity function, detached from the more broadly distributed background population. The sigmas on the fitted Gaussians range from 0.12 to 0.45 magnitudes.

Using the fits to the LMC, SMC and NGC 4258, as given in Paper I, we found that the width of the (single-epoch) IAGB Gaussian distribution to be  $\pm 0.32$  mag. Individual dispersions are given in Column 4 of **Table 1**, and may be useful in determining second-order correlations to the derived distance modulating especially if star-formation history, in the form of significant bursts, are of importance in specific galaxies. That possibility is explored later in this paper.

Tables 6 & 7 contain the following information: [1] Galaxy Name<sup>2</sup>, [2] the TRGB apparent I-band magnitude, [3] the IAGB I-band modal magnitude followed by [4] the one-sigma width of the fitted Gaussian, [5] the number of *IAGB* stars within  $\pm 2$ -sigma of the mode, [6] the sigma on the mean, [7]  $V_{VGS}$  the expansion velocity corrected for Virgo Cluster, Great Attractor and Shapley Supercluster flow perturbations (NED 2023), [8]  $A_I$  the I-band foreground Milky Way extinction (NED 2023), and finally pairs of [8] & [10] true distance moduli and [9] & [11] distances for both the *TRGB* and *IAGB* measurements, assuming  $M_I = -4.05$  and  $-4.64$  mag for the *TRGB* and *IAGB*, respectively.

Figure 1 plots the main result of this paper derived from Table 1. In the figure we give the apparent magnitude of tip of the red giant branch on the horizontal axis, and the apparent mean magnitude of the *IAGB* on the vertical axis. This choice is made so as to make the plot independent of any foreground reddening or any *in situ* extinction that is shared by the two populations, along the same line of sight to the same host galaxy. The run of these two apparent-magnitude values is shown fit by unit slope line, having a zero point that is the mean offset between the two distance indicators. This mean offset (in the sense *TRGB* minus *IAGB*) is  $-0.589$  magnitudes with a scatter of  $\pm 0.119$  mag. The two flanking lines, in the upper plot and in the lower residual plot, are  $\pm 2$  sigma from the unit slope line. Given 92 galaxies in the fit, we calculate an error on the mean of  $0.119/\sqrt{91} = 0.012$  mag. The distribution of residuals is shown as a small inset in the upper left corner of the main panel.

By adopting the independently-determined absolute magnitude for the *TRGB* of  $M_I(\text{TRGB}) = -4.05 \pm 0.035$  (sys.) mag (Freedman 2021), we can then derive the absolute magnitude for the *IAGB* stars, which can be compared to the values derived in Paper I. We find  $M_o(\text{IAGB}) = -4.64 \pm 0.012$  mag, based on 92 galaxies. The value from the independent zero-point analysis in Paper I is identical:  $M_o(\text{IAGB}) = -4.64 \pm 0.116$  mag, albeit with lower statistical significance, being based on only three galaxies, whose individual deviations (LMC:  $+0.156$  mag, SMC:  $-0.023$  mag and N4258:  $-0.133$  mag) all fall well within the 2-sigma ( $\pm 0.24$  mag) bounds of the far-field sample, shown at the bottom of Figure 1.

#### 4. NUISANCE PARAMETERS

It can be asserted that, above and beyond the random noise from measurement errors, the effects of any additional (non-covariant) parameters that can contribute to the scatter seen in Figure 1, will be collectively bounded by the observed scatter of  $\sigma_I = \pm 0.12$  mag, reported for the 92 galaxies so far observed.

A strong contribution to the observed scatter due to metallicity has already been tested for (and not found) using the geometric calibrators discussed in Paper I. That test had only three data points, but each of those galaxies have distinctly different metallicities; moreover they each have accurate geometric distances. No trend of the *IAGB* zero point with metallicity was found.

Here we test for a possible effect of star formation history on the *IAGB*, but, again see no correlation. We have already noted that the width of the Gaussian fit to individual *IAGB* luminosity functions varies over a considerable range of nearly a factor four: from 0.12 to 0.45 mag. It is conceivable that detailed differences in the star formation history over the time period producing the intermediate-age stars that are now populating the oxygen-rich AGB (which are the presumed progenitors of the *IAGB*) could influence the relative numbers of stars at distinct epochs, through bursts or pauses in the star formation rates, revealing themselves in the numbers of intermediate mass stars now entering advanced stage of evolution. Such an activity-modulated weighting of the relative numbers of stars in the oxygen-rich and/or, possibly more importantly, the carbon-rich phase, could result in wider or narrower *IAGB* luminosity functions. Figure 2 attempts to test this possibility.

In Figure 2 we have taken the difference between the true *IAGB* distance modulus of a given galaxy and its true *TRGB* distance modulus, and plotted that difference as a function of that galaxy's *IAGB* luminosity function width. To the eye there is no discernible correlation, as a least squares fit (barely distinguishable from zero in the plot) and its one-sigma bounding slopes (broken lines) around zero, confirm.

Finally, if all of the scatter were to be attributed, say, to differences in internal extinction between galaxies, then this would require  $\sigma(A_I) = \sigma(\text{IAGB}) = \pm 0.12$  mag. This would translate into  $\sigma(E(B - V)) = \pm 0.07$  mag, which is

<sup>2</sup> We note that some of the images used in EDD for TRGB tip detections were primarily intended for the study of disk populations. These galaxies are marked with an asterisk in this table, and the impact of their removal is discussed further in the Appendix

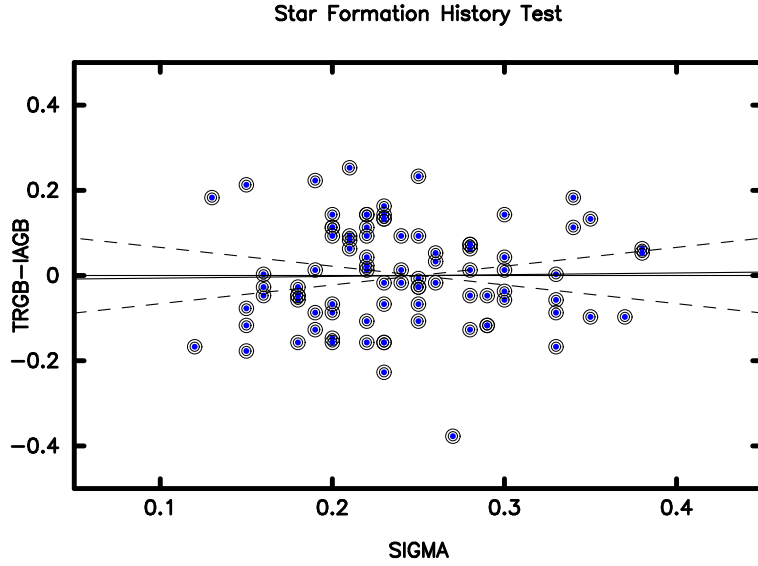


**Figure 2.** Differences between the *TRGB* and *IAGB* true distance moduli as a function of the width of the *IAGB* luminosity function (expressed as a sigma). Broken lines are the one-sigma uncertainties on the statistically flat slope. The lack of a correlation with sigma suggests that star formation history over the age interval sampled by the *IAGB* stars is not perceptibly imprinted on the mode of the *IAGB* luminosity function.

not beyond the realm of possibility. Comparing *IAGB* moduli with *JAGB* moduli for the same galaxies might reveal differential reddening's role here, given that the J-band extinction is a factor of two smaller than extinction measured in the I band. We await *JAGB* distances to significantly more nearby galaxies; HST is fully capable of undertaking this task.

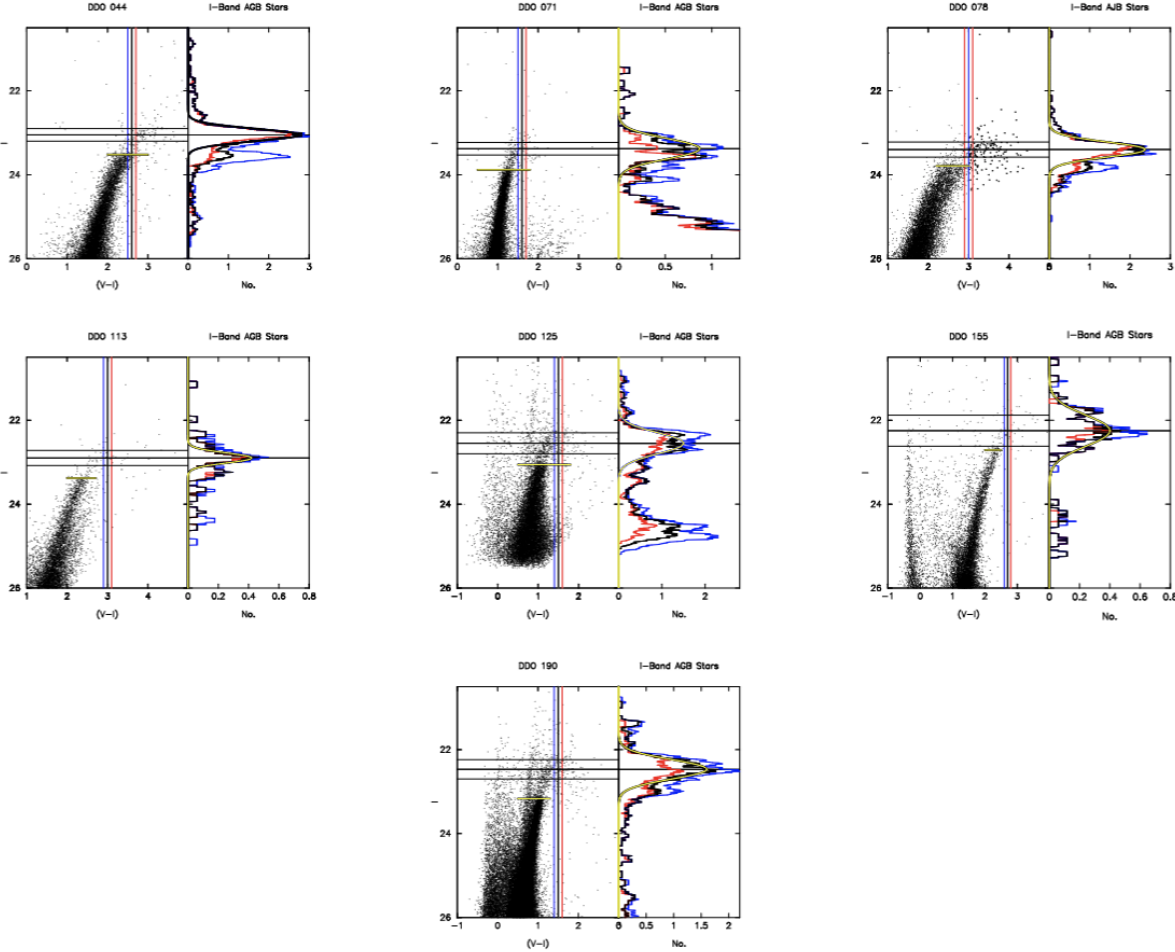


**Figure 3.** DDO Galaxies: I-Band AGB color-magnitude diagrams (left half of each panel) and I-band (F814W) luminosity functions (right half of each panel). Horizontal black lines in the left panel mark the mode of the luminosity function (center line), flanked by lines at  $\pm$  one-sigma in the Gaussian fit to the smoothed luminosity function. A shorter, yellow-on-black line marks the measured level of the TRGB. Thick (smooth) black lines in the right panels are symmetric Gaussian fits to the peak and wings of the smoothed/main luminosity function, also shown in black. Blue and Red luminosity functions correspond to color cuts that are shown in the CMD (left panel) on either side of the adopted color cut (blue vertical line). Blue luminosity functions use the bluer color cut (larger numbers) and the red luminosity functions uses the redder color cut (smaller numbers). See text for additional details.

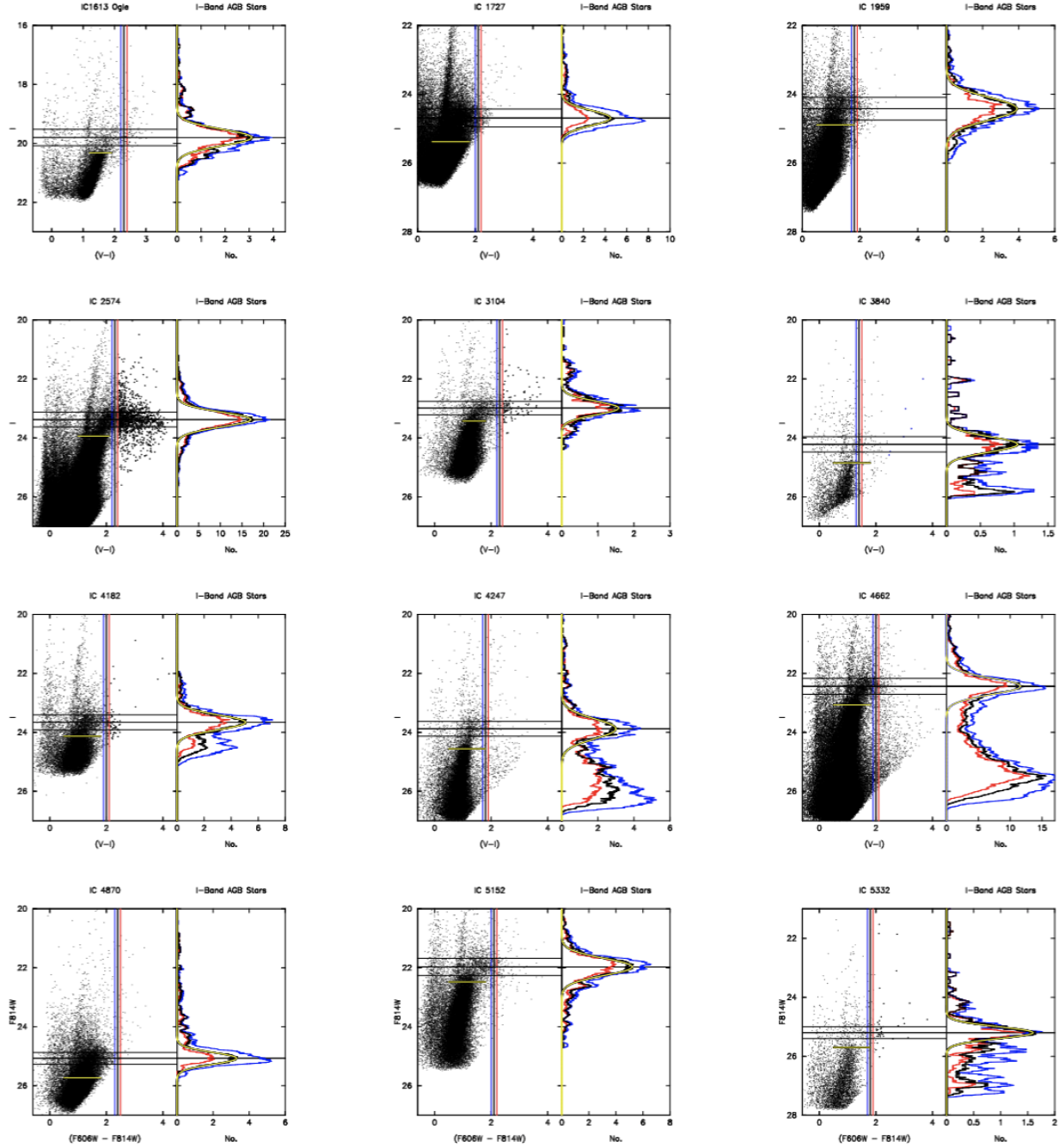


Figure 4. IC galaxies (cont.) See Figure 3 for description.

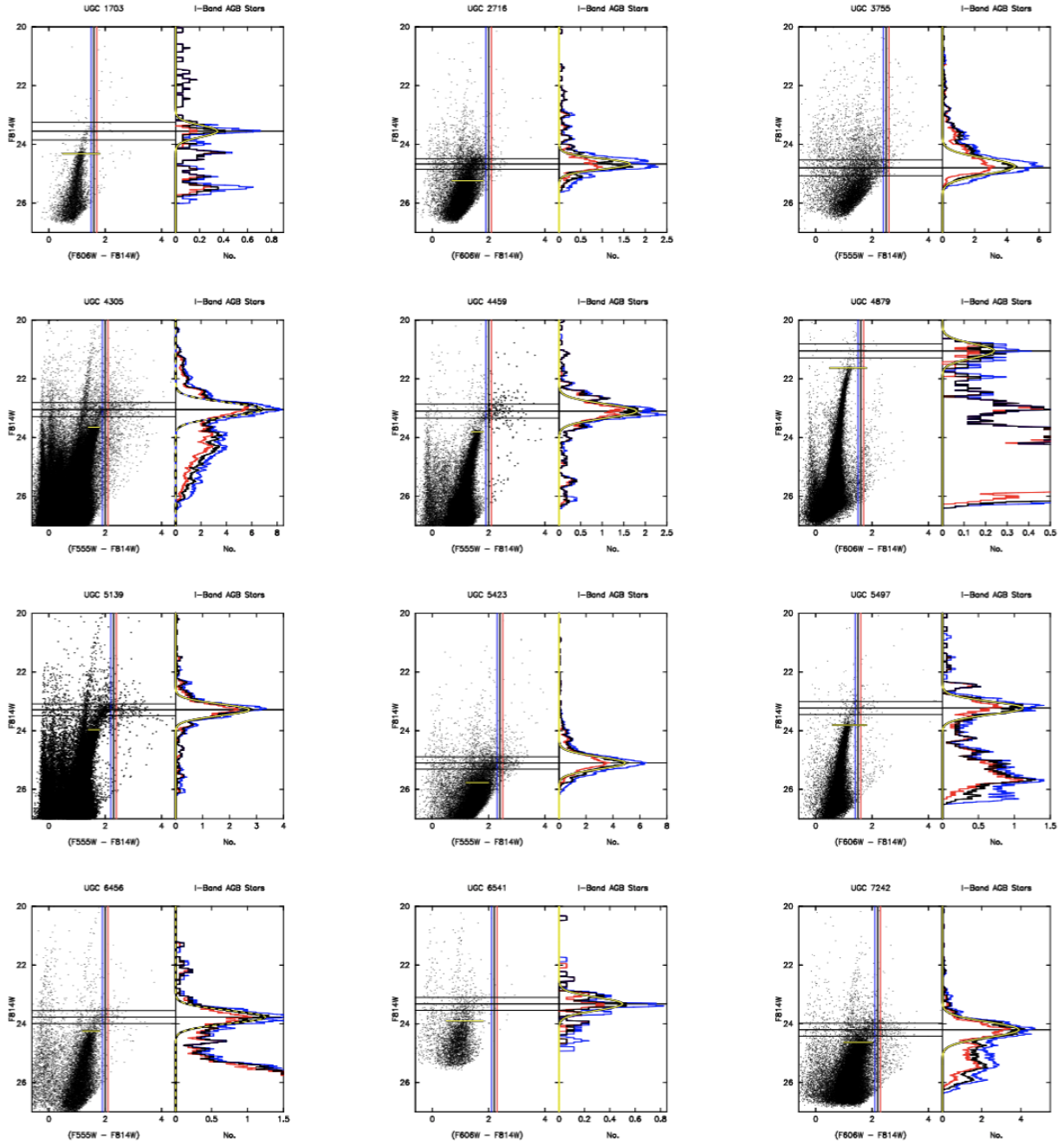


Figure 5. UGC Galaxies. See Figure 3 for description.

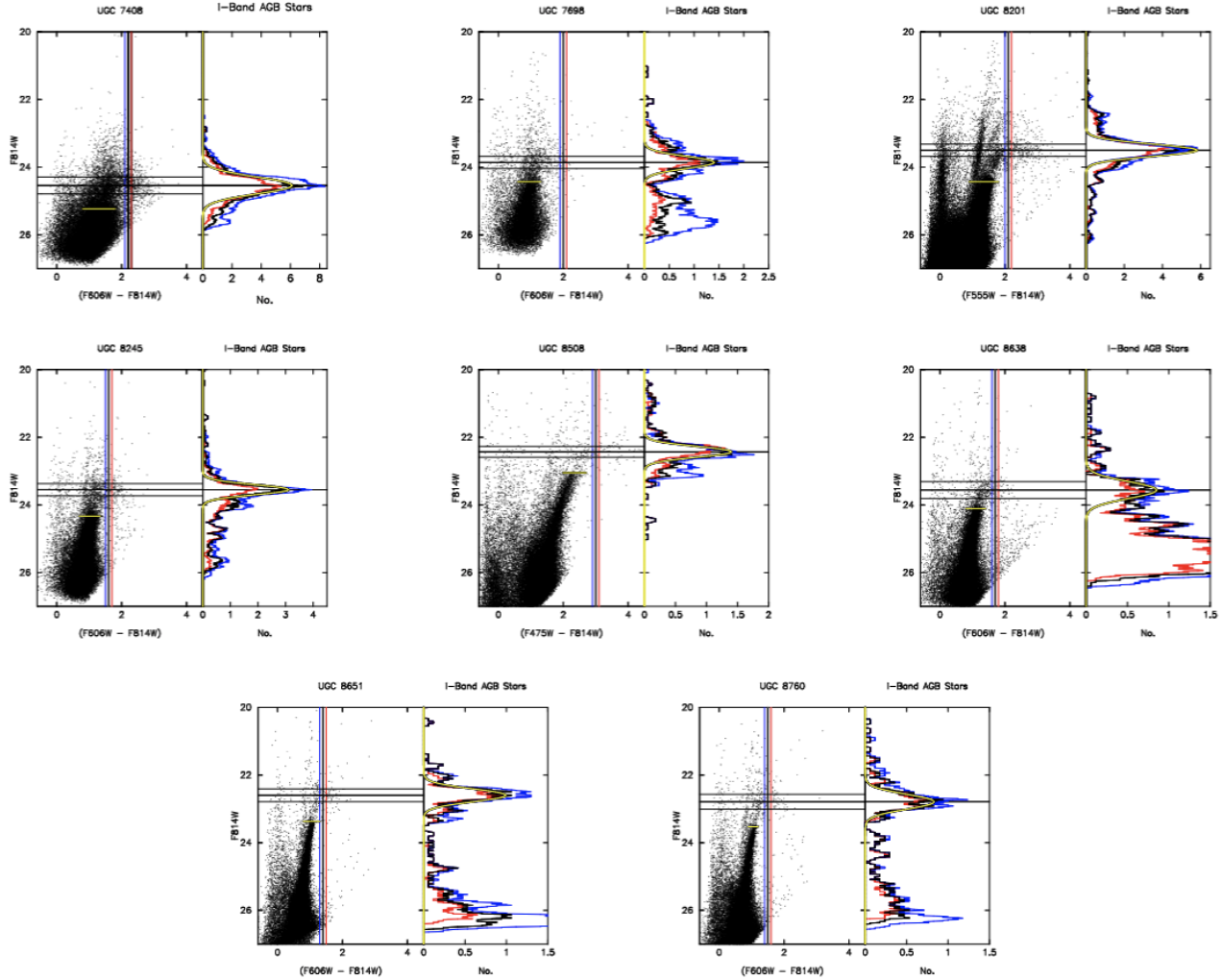


Figure 6. UGC Galaxies (cont.) See Figure 3 for description.

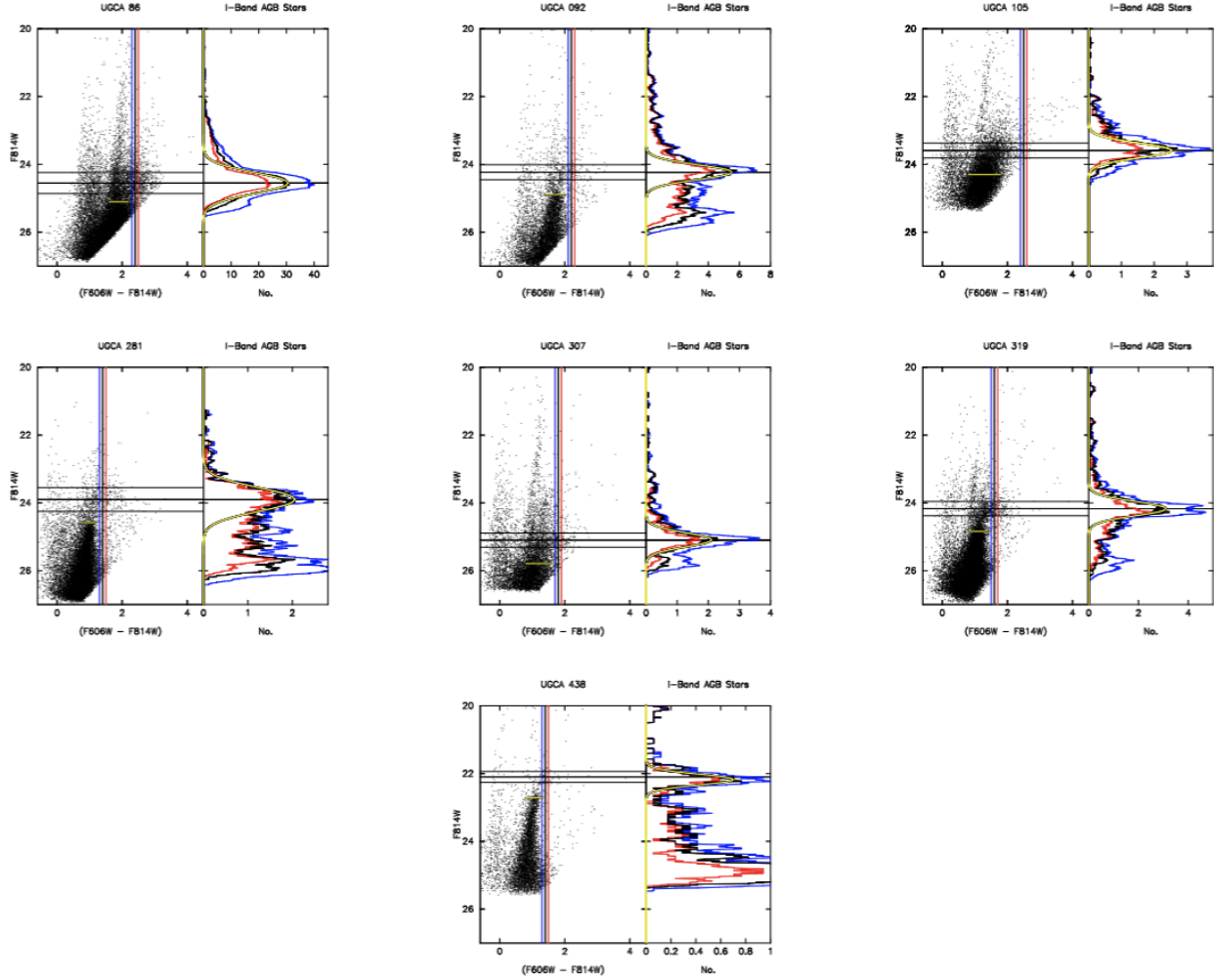


Figure 7. UGCA galaxies. See Figure 3 for description.

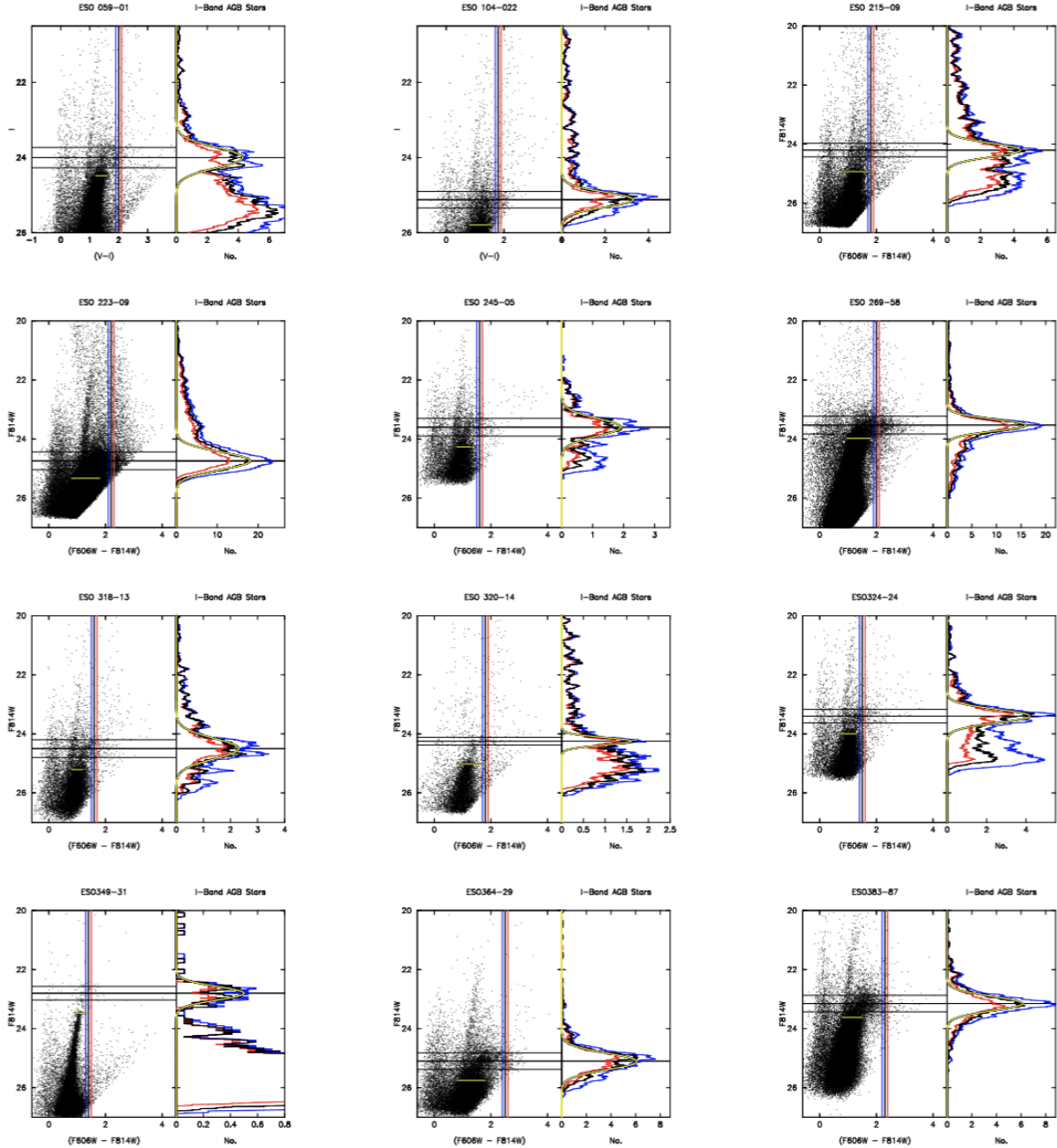


Figure 8. ESO Galaxies. See Figure 3 for description.

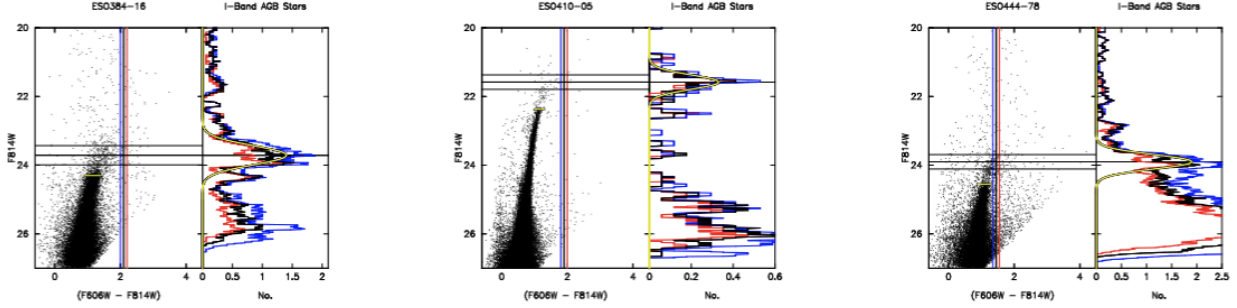


Figure 9. ESO Galaxies (cont.) See Figure 2 for description.

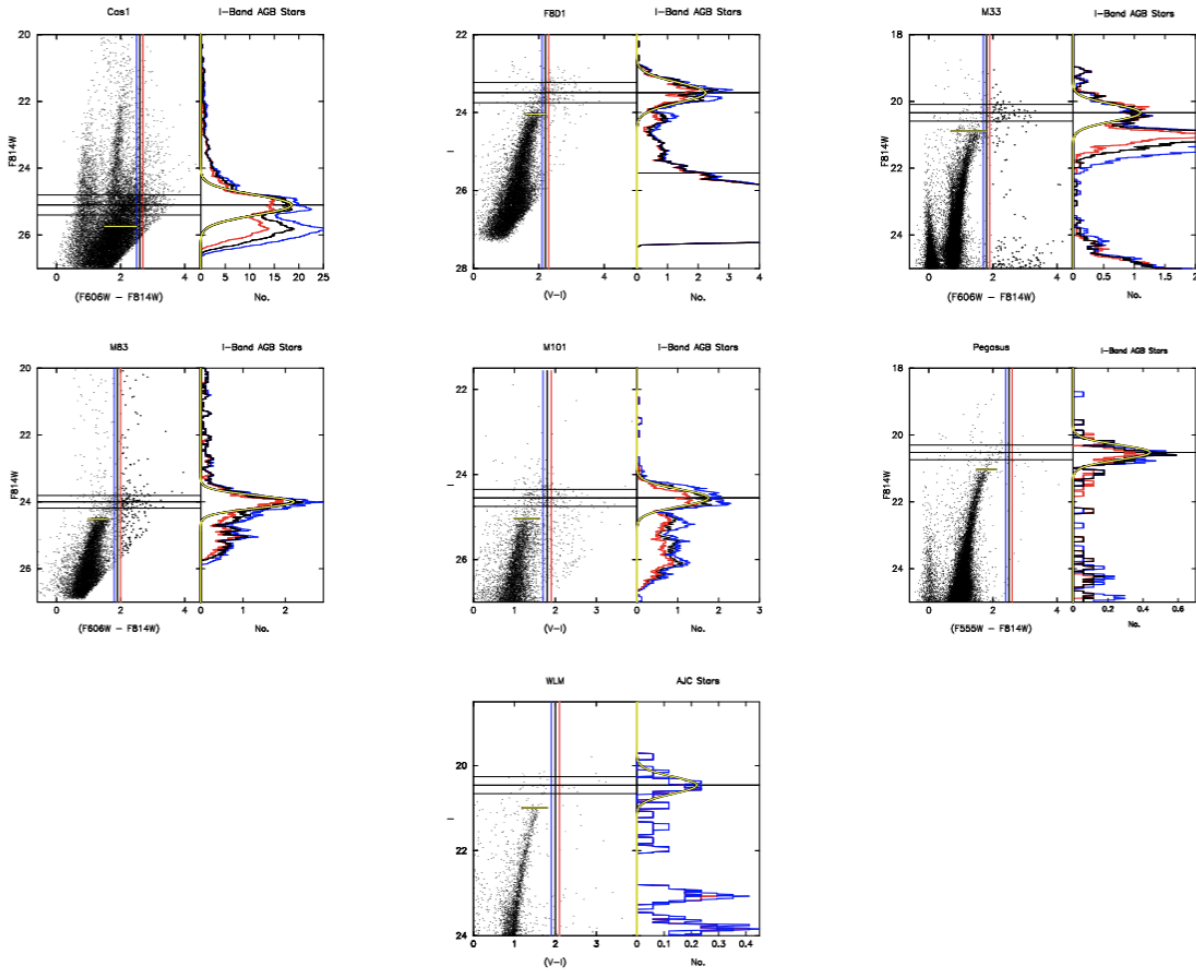
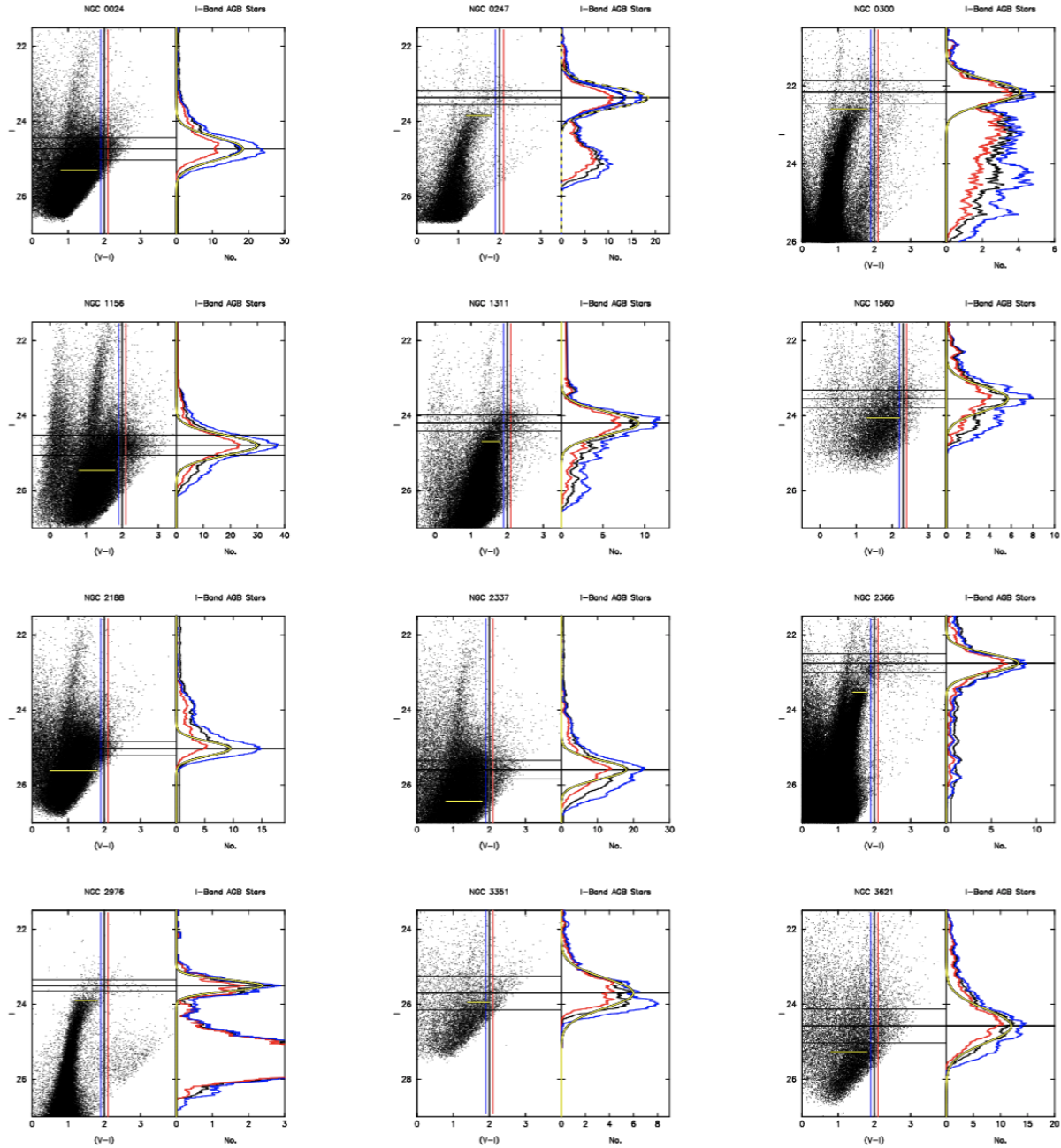


Figure 10. Named Galaxies. See Figure 3 for description.



**Figure 11.** NGC galaxies. See Figure 3 for description.

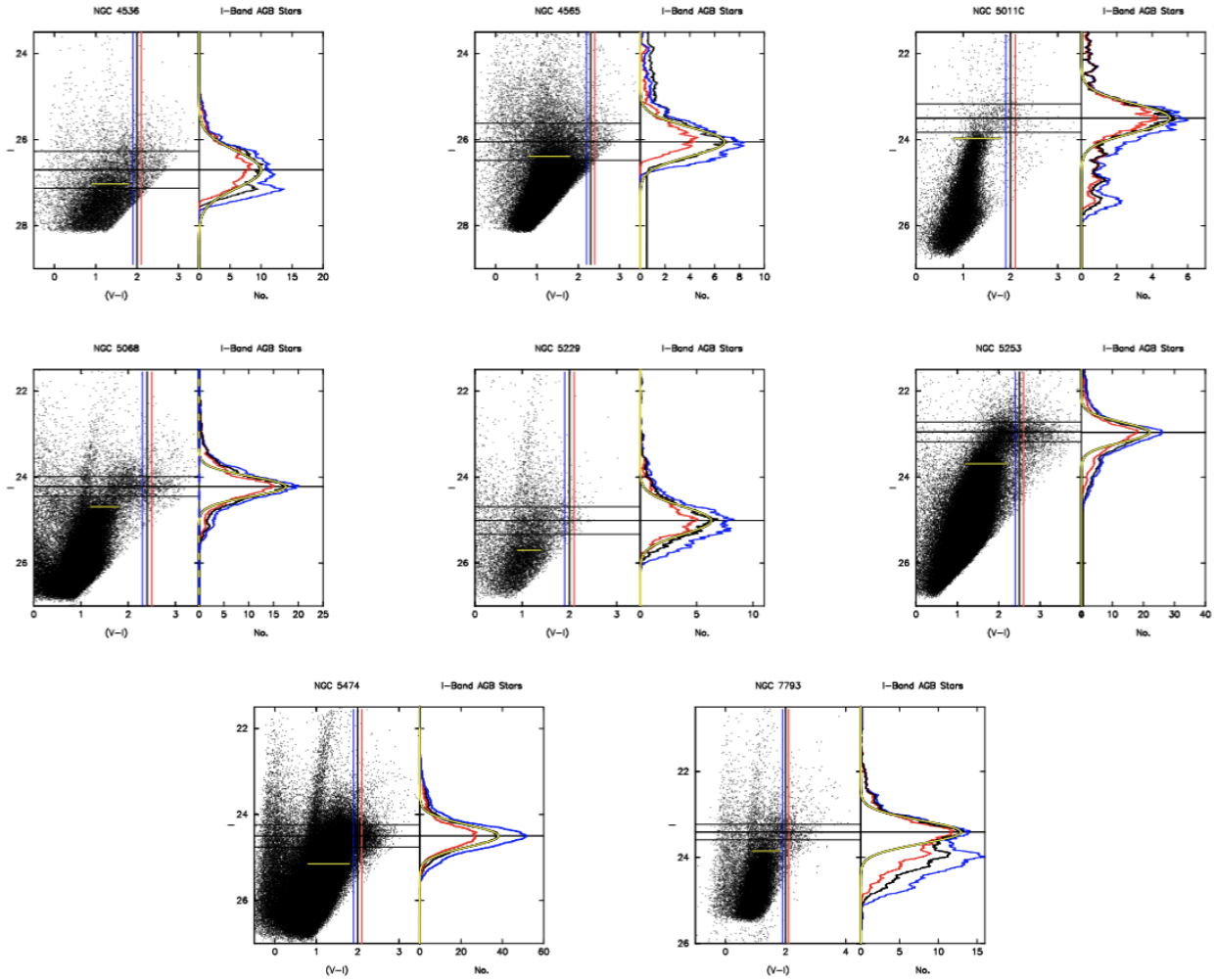


Figure 12. NGC galaxies (cont.) See Figure 3 for description.

**Table 1.** Nearby Galaxies with TRGB and IAGB Distances

Galaxy	I(TRGB)	I(IAGB)	$\sigma$	No.	$\sigma$ (mean)	$V_{VGS}$	$A_I$	$\mu_o$ (TRGB)	D(TRGB)	$\mu_o$ (IAGB)	D(IAGB)
	(mag)	(mag)	(mag)	[5]]	(mag)	(mag)	(mag)	(mag)	(Mpc)	(mag)	(Mpc)
[1]	[2]	[3]	[4]	[6]	[7]	[8]	[9]	[10]	[11]	[12]	
NGC 0024*	25.30	24.73	0.30	2147	0.006	572	0.029	29.32	7.31	29.34	7.38
NGC 0247	23.84	23.37	0.19	1338	0.005	186	0.027	27.86	3.74	27.98	3.94
NGC 0300	22.59	22.15	0.29	405	0.014	109	0.019	26.62	2.11	26.77	2.26
NGC 1156*	25.46	24.79	0.38	1758	0.009	477	0.337	29.17	6.83	29.09	6.58
NGC 1311*	24.69	24.20	0.30	610	0.012	439	0.032	28.71	5.52	28.81	5.78
NGC 1560*	24.06	23.55	0.33	386	0.017	200	0.282	27.83	3.68	27.91	3.82
NGC 2188*	25.61	25.03	0.19	901	0.006	623	0.029	29.63	8.44	29.64	8.47
NGC 2337*	26.43	25.59	0.25	1968	0.006	600	0.131	30.35	11.74	30.10	10.47
NGC 2366	23.53	22.75	0.25	640	0.010	315	0.055	27.53	3.20	27.32	2.91
NGC 2976	23.90	23.50	0.15	130	0.013	167	0.013	27.94	3.87	28.13	4.22
NGC 3351*	25.95	25.70	0.45	813	0.014	659	0.042	29.96	9.81	30.30	11.48
NGC 3621*	25.27	24.58	0.45	2022	0.010	475	0.121	29.20	6.92	29.10	6.61
NGC 4258	25.30	24.69	0.38	329	0.021	600	0.025	29.33	7.33	29.30	7.24
NGC 4536*	27.03	26.70	0.43	1680	0.010	2245	0.027	31.05	16.24	31.31	18.28
NGC 4565*	26.39	26.05	0.23	813	0.012	2021	0.112	30.33	11.63	30.58	13.06
NGC 5011C	23.97	23.50	0.33	441	0.016	600	0.025	27.99	3.97	28.12	4.21
NGC 5068	24.69	24.22	0.23	1178	0.007	452	0.154	28.59	5.21	28.71	5.52
NGC 5128	23.97	23.55	0.12	62	0.015	312	0.173	27.85	3.71	28.02	4.02
NGC 5229*	25.70	25.01	0.34	607	0.014	529	0.027	29.72	8.80	29.64	8.48
NGC 5253*	23.69	22.96	0.23	741	0.008	185	0.084	27.66	3.40	27.52	3.19
NGC 5474*	25.15	24.50	0.26	3750	0.004	481	0.016	29.18	6.87	29.12	6.67
NGC 7793	23.85	23.41	0.18	1184	0.004	237	0.029	27.87	3.75	28.02	4.11
M33	20.89	20.34	0.25	90	0.026	33	0.062	24.88	0.95	24.92	0.96
M83	24.52	24.00	0.19	124	0.017	294	0.101	28.47	4.94	28.54	5.11
M101	25.03	24.57	0.20	130	0.018	455	0.013	29.07	6.51	29.20	6.92
IC 1613	20.32	19.80	0.28	251	0.018	-73	0.038	24.33	0.74	24.40	0.76
IC 1727*	25.38	24.69	0.22	267	0.013	480	0.119	29.31	7.28	29.21	6.95
IC 1959*	24.89	24.42	0.33	351	0.018	508	0.017	28.92	6.09	29.04	6.43
IC 2574*	23.94	23.38	0.25	1202	0.007	238	0.056	27.93	3.86	27.96	3.91
IC 3104*	23.43	22.99	0.23	102	0.023	199	0.617	26.86	2.36	27.01	2.52
IC 3840	24.85	24.22	0.26	75	0.030	358	0.059	28.84	5.86	28.80	5.75
IC 4247	24.56	23.83	0.34	276	0.020	50	0.097	28.51	5.04	28.37	4.72
IC 4662*	23.07	22.44	0.28	914	0.009	164	0.105	27.01	2.53	26.98	2.49
IC 4710	25.40	24.78	0.28	1653	0.007	650	0.134	29.32	7.30	29.29	7.21
IC 4870*	25.73	25.07	0.20	177	0.015	813	0.170	29.61	8.36	29.54	8.09
IC 5152	22.48	21.97	0.29	414	0.014	81	0.038	26.49	1.99	26.57	2.06
IC 5332	25.70	25.20	0.20	89	0.021	708	0.025	29.73	8.81	29.82	9.20
ESO 059-001	24.48	24.00	0.23	27	0.014	297	0.222	28.31	4.59	28.42	4.83
ESO 104-022	25.79	25.12	0.22	178	0.015	729	0.124	29.72	8.77	29.64	8.47
ESO 215-009	24.93	24.20	0.23	342	0.012	322	0.332	28.65	5.37	28.51	5.04
ESO 223-009*	25.33	24.74	0.30	1584	0.008	431	0.391	28.99	6.28	28.99	6.28
ESO 238-005	25.46	24.88	0.29	166	0.023	705	0.020	29.49	7.91	29.50	7.94
ESO 245-005*	24.27	23.60	0.30	145	0.025	309	0.025	28.30	4.56	28.21	4.39
ESO 269-058	23.98	23.53	0.20	905	0.007	1519	0.164	27.87	3.74	28.01	4.00
ESO 318-013	25.21	24.50	0.35	220	0.024	462	0.115	29.14	6.73	29.02	6.36
ESO 320-014	25.02	24.25	0.13	66	0.016	385	0.216	28.85	5.90	28.67	5.42

**Table 1 (continued).** Nearby Galaxies with TRGB and IAGB Distances

Galaxy	I(TRGB) (mag)	I(IAGB) (mag)	$\sigma$ [ $\pm 2\sigma$ ]	No. (mag)	$\sigma$ (mean) (mag)	$V_{VGS}$ (mag)	$A_I$ (mag)	$\mu_o$ (TRGB) (mag)	D(TRGB) (Mpc)	$\mu_o$ (IAGB) (mag)	D(IAGB) (Mpc)
[1]	[2]	[3]	[4]	[5]	[6]	[7]	[8]	[9]	[10]	[11]	[12]
ESO 324-024	24.00	23.40	0.23	263	0.014	280	0.171	27.88	3.77	27.87	3.75
ESO 349-031	23.47	22.80	0.23	30	0.042	224	0.018	27.50	3.17	27.42	3.05
ESO 364-029*	25.75	25.11	0.28	468	0.013	673	0.068	29.73	8.84	29.68	8.63
ESO 383-087	23.62	23.15	0.28	422	0.012	105	0.108	27.56	3.25	27.68	3.44
ESO 384-016	24.30	23.71	0.28	107	0.027	360	0.111	28.24	4.44	28.24	4.45
ESO 410-005	22.37	21.58	0.21	17	0.051	164	0.020	26.40	1.91	26.20	1.74
ESO 444-078	24.55	23.90	0.21	115	0.020	358	0.079	28.52	5.06	28.46	4.92
UGC 02716*	25.24	24.67	0.18	75	0.021	450	0.208	29.08	6.55	29.10	6.61
UGC 01703	24.23	23.55	0.20	14	0.053	217	0.145	28.13	4.24	28.04	4.06
UGC 02716	25.24	24.67	0.18	75	0.020	450	0.208	29.08	6.55	29.10	6.61
UGC 04305	23.65	23.05	0.24	314	0.014	384	0.048	27.65	3.39	27.64	3.37
UGC 04459	23.81	23.10	0.24	134	0.021	184	0.082	27.78	3.59	27.66	3.40
UGC 04879	21.63	21.05	0.24	15	0.062	-14	0.024	25.66	1.35	25.67	1.36
UGC 05139	23.97	23.29	0.20	145	0.017	359	0.024	28.00	3.98	27.91	3.82
UGC 05423	25.77	25.10	0.20	292	0.012	359	0.076	29.74	8.89	29.66	8.55
UGC 05497	23.81	23.23	0.22	66	0.027	378	0.030	27.83	3.68	27.84	3.70
UGC 06541	23.90	23.32	0.22	25	0.044	355	0.028	27.92	3.84	27.93	3.85
UGC 07242	24.63	24.20	0.22	294	0.015	254	0.028	28.65	5.38	28.81	5.78
UGC 07408*	25.23	24.54	0.25	435	0.012	579	0.018	29.26	7.12	29.16	6.70
UGC 07698	24.43	23.86	0.25	69	0.022	277	0.024	28.46	4.91	28.48	4.97
UGC 08201	24.43	23.86	0.18	273	0.011	235	0.024	28.46	4.91	28.48	4.97
UGC 08245	24.33	23.55	0.15	115	0.014	338	0.048	28.33	4.64	28.14	4.25
UGC 08508	23.05	22.43	0.16	65	0.020	208	0.023	27.08	2.60	27.05	2.57
UGC 08638	24.11	23.56	0.25	65	0.031	239	0.020	28.14	4.25	28.18	4.33
UGC 08651	23.37	22.60	0.19	49	0.027	278	0.009	27.41	3.04	27.23	2.79
UGC 08760	23.53	22.79	0.22	49	0.031	261	0.025	27.56	3.24	27.41	3.03
UGCA 086*	25.10	24.55	0.16	2735	0.003	312	1.411	27.74	3.53	27.78	3.60
UGCA 092	24.89	24.25	0.22	362	0.012	103	1.181	27.76	3.56	27.71	3.48
UGCA 105*	24.30	23.59	0.22	105	0.018	328	0.469	27.88	3.77	27.76	3.56
UGCA 281	24.58	23.90	0.35	204	0.025	379	0.022	28.61	5.27	28.52	5.06
UGCA 307	25.79	25.11	0.21	125	0.019	587	0.082	29.76	8.95	29.67	8.59
UGCA 319*	24.84	24.17	0.21	191	0.015	529	0.123	28.77	5.67	28.69	5.47
UGCA 438	22.72	22.18	0.16	29	0.030	94	0.022	26.75	2.24	26.80	2.29
DDO 044	23.52	23.05	0.15	110	0.009	438	0.063	27.51	3.17	27.63	3.36
DDO 071	23.88	23.38	0.15	52	0.021	0	0.148	27.78	3.60	27.87	3.75
DDO 078	23.79	23.40	0.18	120	0.016	230	0.032	27.81	3.64	28.01	4.00
DDO 113	23.38	22.90	0.18	12	0.035	266	0.030	27.40	3.02	27.51	3.18
DDO 125	23.06	22.55	0.25	105	0.024	241	0.027	27.08	2.61	27.16	2.70
DDO 155	22.71	22.25	0.37	37	0.061	109	0.039	26.72	2.21	26.85	2.34
DDO 190	23.17	22.47	0.23	104	0.023	293	0.018	27.20	2.76	27.09	2.62
Pegasus	21.03	20.52	0.22	22	0.156	53	0.102	24.98	0.99	25.06	1.03
Cas 1	25.74	25.10	0.30	1652	0.007	312	1.532	28.26	4.48	28.21	4.39
F8D1	24.04	23.49	0.26	155	0.021	10	0.163	27.93	3.85	27.97	3.93
SMC	14.93	14.37	0.33	999	0.010	0	0.060	18.92	0.06	18.95	0.06
WLM	20.99	20.46	0.20	11	0.060	-14	0.057	24.98	0.99	25.04	1.02

#### 4.1. *Color Magnitude Diagrams*

Figures 3 through 14 contain the color-magnitude diagrams to the left within each sub-panel, for the galaxies with *IAGB* distances derived in this paper. The right side of each sub-panel contains the marginalized luminosity function (oscillating black line) for those stars with colors in excess of the vertical black line shown in the CMD. The blue curve is a Gaussian fit in height and width to the core of the luminosity function. Red lines to either side of the adopted black luminosity function are the luminosity functions resulting from perturbing the color cut by  $\pm 0.10$  mag, given to illustrate the sensitivity of the luminosity function to changes in the color selection function.

## 5. SUMMARY AND CONCLUSIONS

Following the introduction and zero-point calibration of a new method of determining extragalactic distances (Madore et al. 2024) using I-band Asymptotic Giant Branch *IAGB* stars, we have undertaken an exploratory extended application out to 9 Mpc. I vs (V-I) color-magnitude diagrams for 92 galaxies, have been used to determine (a) the apparent I-band (F814W) magnitude of the TRGB and (b) within the same diagram, for the same galaxies, determine the I-band modal magnitude of the very reddest population of high-luminosity stars, the *IAGB* stars. From this comparison it is found that the *IAGB* stars are -0.589 mag brighter than the TRGB, where the standard error on that difference is  $\pm 0.119$  mag. Dividing the contributions to this cumulative error equally between the two distance indicators suggests that they would both have intrinsic dispersions of  $\pm 0.084$  mag in that case. This is probably high for the TRGB, suggesting that a more equitable estimate might be  $\pm 0.06$  mag for the *TRGB* and  $\pm 0.10$  mag for the *IAGB* at this early stage in its application. The effect of differences in the star formation histories, differences in the mean metallicities of the AGB populations, and differences in the *in situ* reddening between galaxies in this sample must be contained within the 0.10 mag scatter cited above, as found in the comparison of TRGB and IAGB distance moduli.

The total error on the intercomparison yields an error on the mean between the two distance indicators of  $\pm 0.012$  mag. This relative distance zero point can be used to provide an independent calibration of the *IAGB* distance determination method. Adopting  $M_I(\text{TRGB}) = -4.05$  mag for the tip of the red giant branch stars gives  $M_I(\text{IAGB}) = -4.64$  mag  $\pm 0.012$  (stat)  $\pm 0.02$  (sys).

We **close by noting** that the data used for this study were not taken with the purpose of measuring *IAGB* distances, and that further targeted observations taken with consistent instrumentation and calibrations will improve future applications. Thus, with single-epoch observations (using HST and/or Roman), it is reasonable to expect that these stars will be capable of independently measuring the distances to the majority of the Type Ia supernova calibrating galaxies (i.e., within 40 Mpc) currently forming the basis for determining the local value of the expansion rate of the universe. Using NIRCam and its F090W filter, JWST should be able to apply the method even further.

## ACKNOWLEDGMENTS

The data presented in this paper were obtained from the Extragalactic Distance Database (EDD). We thank the *University of Chicago* and the *Observatories of the Carnegie Institution for Science* for their support of our continuing research into the calibration and determination of the expansion rate of the Universe.

*Facility:* HST (ACS/WFC, WFC3/IR)

## 6. REFERENCES

- Freedman, W.F. 2021, ApJ, 919, 16
- Freedman, W.F. & Madore, B.F. 2023, JCAP, 11, 50, arXiv.2309.05618
- Freedman, W. L., Madore, B. F., Hoyt, T., et al. 2020, ApJ, 891, 57
- Hoyt, T.J., 2023, NatAs, 7 590
- Graczyk, D., Pietrzyński, G., Thompson, I. B., et al. 2014, ApJ, 780, 59.
- Lee, A. 2023, ApJ, 956, 15
- Madore, B.F., Freedman, W.L., Hoyt, T.J., et al. 2025, ApJ, in press, (Paper I)
- Pietrzyński, G., Graczyk, D., Gallenne, A., et al. 2019, Nature, 567, 200.
- Reid, M. J., Pesce, D. W., & Riess, A. G. 2019, ApJL, 886, L27
- Skowron et al. 2022
- Scowcroft, V., Freedman, W. L., Madore, B. F., et al. 2016, ApJ, 816, 49.
- Wu, J., Scolnic, D., Riess, A.G., et al. 2023, ApJ, 954, 87

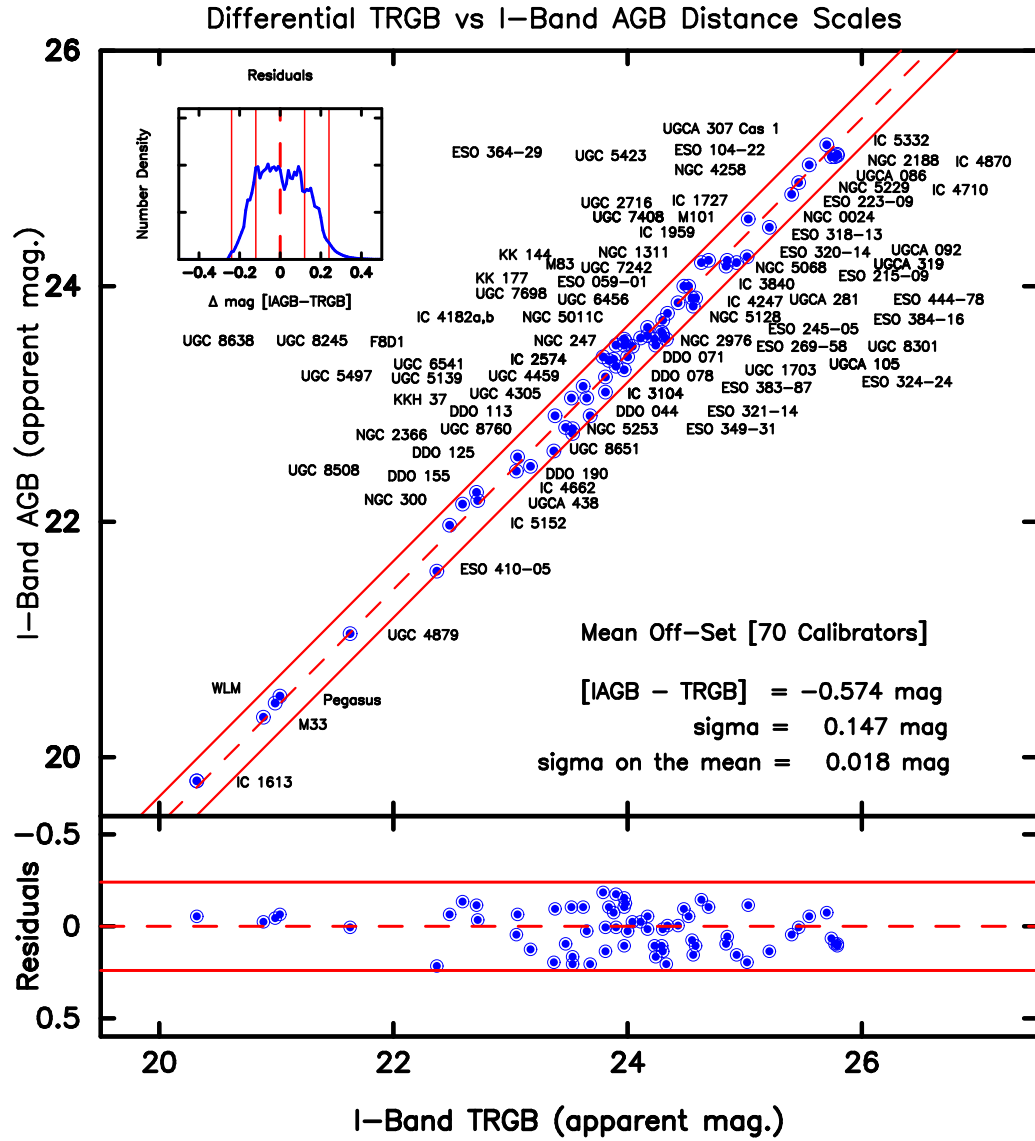


**Figure 13.** Same as Figure 1 except this sample has been down-selected to remove 23 galaxies that were deemed to be sub-optimal for TRGB measurements based on the placement of their points largely in the disks of these galaxies.

## 7. APPENDIX

### 7.1. *Analysis of a Down-Selected Subsample of 70 Galaxies*

A number of the galaxies discussed in the main paper above had their original pointing concentrated on the disks of the target galaxies and, they are therefore less than optimal for detecting and measuring the halo TRGB population. The names of those 22 galaxies are marked with a following asterisk in Table 1, and an inspection of their CMDs bear witness to the significant presence of Population I stars in the form of blue and red supergiants.

Figure 16 shows the resulting correlation of I-Band AGB distances versus I-Band TRGB distances for the remaining 70 down-selected galaxies. The quantitative changes in the correlation are small, and perhaps slightly counter-intuitive. The mean difference [IAGB-TRGB] has become less negative (-0.574 mag for the smaller sample as compared to -0.589 mag for the larger sample) suggesting that the TRGB population superimposed on the disks that were dropped from the sample, were (as might have been anticipated) biasing the solution towards brighter magnitudes. On the other hand, drawing down the bias by rejecting the (potentially) crowded TRGB sample results in a net increase in the scatter around the mean, with it going from  $\pm 0.119$  mag up to  $\pm 0.147$  mag. One might have predicted that the scatter would decrease in removing a biased subset of the data, but it did not.